The International Journal of Advanced Manufacturing Technology (2022) 123:2655–2667
https://doi.org/10.1007/s00170-022-10317-w

ORIGINAL ARTICLE

Airborne acoustic emission of an abrasive waterjet cutting system as means for monitoring the jet cutting capability

Edoardo Copertaro[1] · **Massimiliano Annoni**[2]

Received: 13 June 2022 / Accepted: 11 October 2022 / Published online: 3 November 2022
© The Author(s) 2022

Abstract

Abrasive waterjet cutting is a manufacturing technology making use of a high-speed waterjet with abrasive particles in suspension, for cutting materials with different mechanical properties. Product quality requirements are pushing towards an improvement of tracking and stabilization methods of the relevant process variables. Amongst those, the jet kinetic power defines the cutting capability and has a significant impact on the final cut features. This variable is subject to relevant fluctuations versus time. Besides, the current state of the art does not provide means for its in-line monitoring. The aim of this contribution is to monitor the airborne acoustic emission of an abrasive waterjet cutting head and investigate its correlation with the jet kinetic power. The investigation is carried out by means of factorial studies, in which the jet is fired at various water pressures and abrasive feed rates, providing different kinetic powers. The acoustic emission is synchronously monitored by means of a condenser microphone, installed on the cutting head. Data at frequencies above 40 kHz is found to constitute a robust and selective acoustic signature of the airborne jet. The acoustic signature is proven to be an effective in-line indicator of the jet kinetic power and its pressure-induced variations, whilst abrasive-induced variations remain undetected. A calibration procedure is presented, for translating the acoustic data into a jet kinetic power. The method is validated by means of further experiments that envisage its deployment in a real scenario. Overall, the presented method constitutes a robust tool for monitoring pressure-induced variations of the jet cutting capability.

Keywords Abrasive waterjet cutting · Acoustic emission · Process monitoring

Nomenclatures

p	Water pressure
ρ	Water density
m_a	Abrasive mass flow rate
v_{th}	Pure waterjet theoretical incompressible velocity
$v_{th,c}$	Pure waterjet theoretical compressible velocity
v_j	Pure waterjet real velocity
v_a	Abrasive waterjet velocity
ψ	Compressibility coefficient
c_c	Contraction coefficient
c_v	Velocity coefficient
c_d	Discharge coefficient
m_w	Water mass flow rate
Q_w	Water volumetric flow rate
P_{part}	Kinetic power of the abrasive particles inside the jet
S_j	Jet cross-sectional area at the *vena contracta*
d_n	Orifice nominal diameter
S_n	Orifice nominal cross-sectional area
r_d	Abrasive loading ratio

✉ Massimiliano Annoni
massimiliano.annoni@polimi.it

[1] Faculté Des Sciences, de La Technologie Et de La Communication, Université du Luxembourg, Avenue de L'Université, Esch-sur-Alzette L-4365, Luxembourg

[2] Dipartimento di Meccanica, Politecnico di Milano, Via Privata Giuseppe La Masa 1, Milan 20156, Italy

1 Introduction

Abrasive waterjet cutting (AWJC) is acknowledged as a leading manufacturing technology in numerous high-end applications (e.g. aerospace, defense, automotive). AWJC is characterized by several interesting features including its relatively low initial investment, no heat-affected zone on the workpiece, no limitations in shape complexity, the absence of mechanical contact with physical tools making it very delicate on fragile and/or composite materials, narrow kerf (down to 0.3 mm), negligible burrs and good edge sharpness [1]. All these features provide an edge with respect to alternative technologies.

However, power-user segments require cutting-edge performances from their manufacturing processes, in terms of stability and product assurance, to tackle very stringent safety and quality standards. Indeed, complying with such requirements is a relevant challenge for AWJC, because of unstable process conditions and limited monitoring and control capabilities of current machines [2]. The present investigation lies in the field of vibroacoustic process monitoring, as a means for extracting relevant information that could benefit AWJC in these instances.

The cutting head, i.e. the terminal component of an AWJC system, is responsible for guiding the cutting jet towards the workpiece and is shown in Fig. 1: water is fed and controlled by means of an intensifier or direct drive pump with pressure typically ranging between 300 and 400 MPa, although pumps up to 600 MPa are available nowadays. The water flows through the primary orifice and here pressure is converted into kinetic energy, producing a high-speed (about 1000 m/s) waterjet. Downstream, the mixing chamber receives a mixture of abrasive particles and air, at a rate that typically ranges between 100 and 400 g/min (although lower rates can be used in high-precision applications [3], down to 3–5 g/min) and is controlled by various types of feeders (belt-based, screw-based and others). The resulting multiphase jet flows through the focusing tube, which is responsible for transferring momentum from the water to the particles. After leaving the focusing tube, the multiphase jet gets airborne and subsequently impacts on the workpiece, resulting in a material removal process [4].

In AWJC, the Computer Numerical Control (CNC) software is responsible for controlling several process variables,

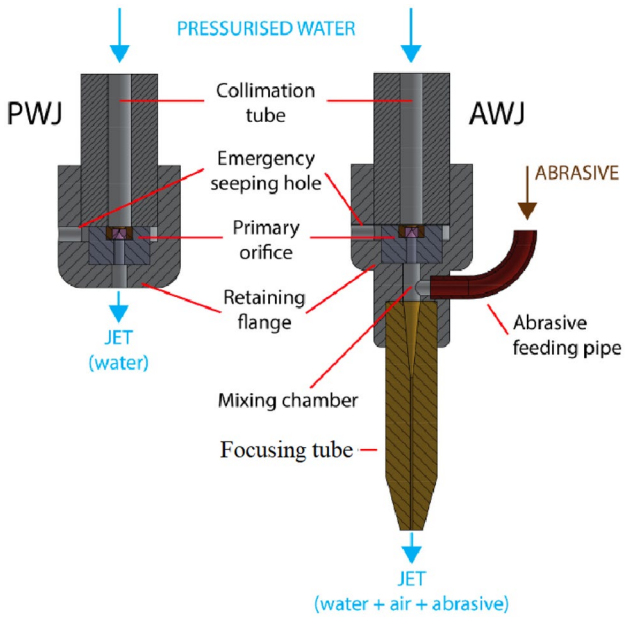

Fig. 1 AWJC head (PWJ: pure waterjet; AWJ: abrasive waterjet) [3]

the most relevant being the water pressure (p), the abrasive feed rate (m_a), the traverse speed (or feed rate) and the standoff distance. The standoff distance is the distance between the focusing tube's tip and the workpiece; it is typically maintained between 1 and 2 mm, which constitutes the optimal range for most of the applications. The traverse speed, p and m_a are selected according to CNC performance models that are designed for maximising productivity; more in detail, the traverse speed is generally pushed to the highest value that complies with the target quality of the kerf walls (basically the surface roughness and the kerf taper), whilst the p and m_a setpoints correspond to the maximum values that can be delivered by the hardware.

The kinetic power P_{part} is an important variable that defines the cutting capability and has an impact on several process Key Performance Indicators (KPIs) [5]. This variable becomes even more critical in applications requiring top-notch accuracy and absolute integrity of the cutting edge, e.g. no cracks on fragile materials. The theoretical definition of P_{part} corresponds to the kinetic power of the abrasive particles, being the only phase that contributes to the material removal process. The theoretical derivation of P_{part} is reported in Sect. 2 of the present paper, as well as its correlation with p and m_a, which are the two process parameters that are used for its control. Machine builders have delivered substantial efforts for stabilizing P_{part}, in an attempt to improve productivity and the final product quality. Indeed, further variables besides p and m_a concur to its fluctuation and drift versus time; these include the instantaneous fluid-dynamic conditions inside the mixing chamber, which tend to fluctuate, the instantaneous feeding rate from the abrasive line [6], which is affected by a relevant instability, and the instantaneous focusing tube's inner diameter, which increases due to the wear phenomena occurring [7, 8], as it accumulates operating hours. Disposing of an in-line P_{part} indicator available could enable the implementation of closed-loop controls of p and m_a specifically aimed at compensating said fluctuations. Unfortunately, the monitoring infrastructure of current AWJC machines cannot deliver this information. Such deficiency has pushed the research towards the implementation of innovative monitoring techniques that can enrich the available process dataset. The present investigation is intended to demonstrate how the AWJC airborne acoustic emission can be used for extracting a selective and robust acoustic signature of the waterjet, from which an in-line P_{part} indicator can be derived. The subsequent part of this section presents a literature survey about vibroacoustic process monitoring, with a focus on AWJC applications.

1.1 Literature survey

The AWJC operational vibroacoustic emission has been the object of several studies, aimed at extracting relevant process information. The literature survey indicates that these

methods can be categorized into two groups: a first, in which the objective is to monitor process and workpiece variables, including the final quality; a second, with a specific focus on the diagnostics and condition monitoring of components.

The first category of methods relies on the extraction of synthetic indicators from the monitored signals in various domains (time, frequency, wavelet), which are proven to correlate with the target variables. Several of these methods are specifically intended to provide an indirect estimation of the workpiece quality, i.e. the surface roughness and/or the cutting depth, starting from the in-line vibroacoustic data monitored at various positions, either on the machine or the workpiece itself. In [9], the authors analysed the acoustic emission during AWJC of AISI 1018 carbon steel, with the aim of monitoring the instantaneous cutting depth. Measurements were carried out by means of two acoustic sensors attached on the workpiece, in the proximity of the cutting area, and the signals' root mean square (RMS) linear correlation with the cutting depth was subsequently proven. In [10] the authors used four accelerometers for measuring an AISI 309 stainless steel workpiece vibration, during AWJC operations at various m_a, finding a correlation between the workpiece quality and certain spectral amplitudes. In [11], the authors measured the operational acoustic emission during AWJC operations and in the proximity of the cutting head; subsequently, the signals' correlation with the transverse speed was proven, thus enabling the implementation of a system for closed-loop control and supervision over the workpiece quality. In [12], the authors carried out AWJC experiments on aluminium 5251 panels, at different traverse speeds, and assessed the impact of this parameter on the surface quality, by means of off-line measurements; synchronously, the acoustic emission originated from the workpiece was measured at very high frequencies (up to 1 MHz) and recorded. Subsequently, the signals were analysed in the frequency domain, finding a correlation with the surface quality. The AWJ drilling of Inconel 718 and AISI 1040 steel was the object of experimental investigation in [13]; here the authors successfully proposed the operational acoustic emission as a tool for monitoring the penetration depth, as well as characterizing the type of worked material. The same method was also proven effective in identifying non-compliant worked pieces, by means of comparison against benchmark acoustic data. In [14], the cutting head's vibration was measured by means of an accelerometer, during cutting experiments on a titanium-alloy workpiece carried out at various p, m_a, standoff distances and traverse speeds. At the same time, the slot depth was measured by means of an optical microscope. In a first step, the optical measures allowed to correlate the kerf characteristics with said process parameters; subsequently, a correlation between the slot depth and the measured vibration amplitude was proven.

Other contributions are more focused on the extraction of indicators of process variables (e.g. p, m_a, the traverse speed, the standoff distance) that could provide the ground for new control strategies aimed at improving process control and stability: in [15], AWJC experiments were carried out on aluminium alloy sheets using various standoff distances and maintaining the other process parameters constant. The operational acoustic emission was monitored by means of a microphone; the signal processing consisted in the computation of two indices, namely the RMS and a power spectrum integral, both of which were proven to be linearly proportional to the standoff distance, for limited thicknesses of the workpiece. In [16], an analogous experimental setup to the one of [10] was used for demonstrating the correlations of the workpiece vibration with m_a, the transverse speed and the focusing tube's inner diameter. In [17], the authors carried out an experimental investigation, in which Composite Fiber-Reinforced Panel (CFRP) materials were cut by means of AWJC and the acoustic emission monitored by means of two sensors, of which one installed on the cutting head and the other on the workpiece. In the conclusions, the authors observed a correlation between the transverse speed (hence the surface roughness) and the signals' amplitudes. In [18], AWJC experiments on CFRP, titanium and CFRP-titanium stacks were carried out, with the aim of correlating the vibroacoustic emission with p and the traverse speed. This investigation was successful in identifying frequency ranges with a detectable sensitivity to the target variables; amongst further conclusions, the authors mentioned the possibility of exploiting this method in innovative strategies for process control and troubleshooting. In [19], AWJC of titanium-CFRP stacks was carried out at various p and m_a, whilst the operational acoustic emission was monitored and processed by means of a wavelet decomposition method. Amongst the conclusions, the time-localized feature of the wavelet filters was proven to be effective in extracting relevant process information from the signals.

Further investigations specifically tackle the correlation of operational vibroacoustic emission with energy performance indicators of the AWJC process. Herein, the target KPIs mostly consist in the jet input energy and its active fraction, i.e. the amount that provides an effective contribution to the cutting process (hence correlates with the cutting depth). In [20] a first attempt in the direction is presented, in which a monitoring setup consisting of two acoustic sensors at different locations was successfully exploited for monitoring the active energy, as well as delivering a penetration depth estimator and further troubleshooting data. An analogous study is reported in [21]: here a similar setup was used for measuring the active energy and the information exploited in a subsequent step, for feeding innovative closed-control loops of p and m_a.

The AWJC operational vibroacoustic emission has been exploited as a source of relevant information for process diagnostics and condition monitoring, as well. In [6], the authors

assert that information can be extracted from the monitored signals, which is related with the health status of the primary orifice and the focusing tube. The prior-art shows a variety of methods relying on AWJC operational vibroacoustic emission and dealing with the monitoring of wear progression. The investigations reported in [22, 23] and [24] were specifically intended to correlate the focusing tube's wear status with the AWJC operational acoustic emission. Herein, experimental campaigns were carried out by using focusing tubes with different inner diameters and measuring the operational acoustic emission, which was subsequently analysed in the frequency domain. In the conclusions of the studies, a frequency range was identified at about 20 kHz, in which the power spectral amplitudes were proven to be sensitive to the focusing tube's inner diameter. In [25] a further experimental study that deals with the monitoring of the focusing tube's wear status and makes use of a setup analogous to the one used in [16] is presented, consisting of four accelerometers attached to the workpiece. Vibration signals were gathered during AWJC operations and analysed in the frequency domain. In the conclusions, the authors identified characteristic spectral peaks and demonstrated their sensitivities to both the focusing tube's inner diameter and m_a. In [26], the structure-borne acoustic emission of an AWJC nozzle was measured at various operating hours and by means of a contact sensor installed on its outer surface, finding a correlation between the signal's RMS and the wear progression, as well as the integrity status. In [7], the AWJC operational vibration was monitored by means of one accelerometer installed at the focusing tube's tip and the signal exploited for tracking the focusing tube's first resonant frequency, the latter proven to constitute an effective wear status indicator.

1.2 Research gap and motivation of the present work

The outlined literature survey seems to confirm the effectiveness of vibroacoustic monitoring as a means for extracting relevant process information that could help in tackling the current AWJC limits and issues. In [5] one further setup is discussed, which appears particularly relevant to the aim of the present dissertation: here the authors made use of a special focusing tube, hosting two accelerometers on its tip; an experimental study was conducted, in which the jet was fired at various p and m_a. The operational vibration was monitored by means of the two accelerometers, and subsequently analysed in the frequency domain. A hypothesis was made, in which one particle impact in the focusing tube's inner bore triggers a single vibration response that is quantitatively proportional to the particle's kinetic energy and the overall vibration is the sum of the single responses per unit of time. The hypothesis was confirmed by the correlation of the high-frequency vibration amplitude with P_{part}, notably above 10 kHz; a much lower correlation was found at lower frequencies. The discriminant factor amongst the two frequency ranges was identified in the types of vibration modes involved: whilst the high-frequency range only includes local modes of the focusing tube, the low-frequency range appears affected by global modes of the AWJC system, which do not bring relevant information for the purpose of P_{part} monitoring. Indeed, the method detailed in [5] was proven effective in delivering a reliable P_{part} in-line indicator. However, the method relies on the deployment of sensing hardware at the very tip of the focusing tube, which constitutes a critical location, given its proximity to the jet impinging point. On the other hand, a method based on a sensors' deployment further away from the jet could represent a more robust and user-friendly setup from the end-user perspective, hence providing greater potential for market success.

In the present investigation, the authors intend to monitor P_{part} by means of the airborne acoustic emission, measured with a condenser microphone installed on the cutting head. Factorial studies are presented, in which p and m_a are varied amongst different set points and the acoustic emission monitored and processed in the frequency domain. The monitoring setup appears much simpler compared to [5] as it does not require the installation of contact sensors, as well as more robust, being the microphone located further away from the jet impinging point. Conclusions of this study are partially coherent with [5] as a robust correlation between P_{part} and the measured acoustic emission is found, above 40 kHz. Such high-frequency data is proven to constitute a robust and selective acoustic signature of the airborne jet, relatively unaffected by input disturbances and with good measurement reproducibility. Overall, the presented method appears effective in monitoring p-induced variations of P_{part}, whilst the impact of m_a remains undetected. The method is expected to represent a valuable tool for supporting innovative closed-loop controls of the water pump, which could help in tackling the end-user requirements for improved process stability.

The present contribution is structured as follows: in Sect. 2, the theoretical definition of P_{part} is presented; in Sect. 3, the materials and methods are introduced; in Sect. 4, results are presented and discussed; and conclusions are drawn in Sect. 5.

2 Theoretical definition of the jet kinetic power

The jet kinetic power P_{part} can be derived from the typical relationships existing amongst the AWJC variables, which are taken from [4]. The Bernoulli equation (Eq. 1) provides the theoretical waterjet velocity v_{th}, from the pressure conversion

into kinetic energy taking place through the primary orifice, assuming no energy losses occur in the process and water incompressibility. The water compressibility plays a significant role at the very high pressures of AWJC applications; the theoretical compressible velocity $v_{th,c}$ is expressed in Eq. 2, which is derived from Eq. 1 and takes the water compressibility into consideration by introducing the two constants C and L; a coefficient ψ can be introduced for capturing the water compressibility, being defined as the ratio between $v_{th,c}$ and v_{th}. A further coefficient c_v accounts for the energy losses occurring through the primary orifice. The real jet velocity v_j can be expressed starting from v_{th} and by means of the two coefficients ψ and c_v (Eq. 3). In Eq. 4, the water volumetric flow rate Q_w is expressed as the product of v_j and the jet cross-sectional area at the *vena contracta* S_j; the contraction coefficient c_c is the ratio between S_j and the nominal cross-sectional area of the primary orifice S_n; the discharge coefficient c_d is defined as the product of the three coefficients c_v, c_c and ψ. Assuming that the coefficient c_d for a certain primary orifice is known, the water mass flow rate m_w can be expressed as the product of c_d, S_n, v_{th} and the water mass density ρ (Eq. 5). The abrasive loading ratio r_d is defined in Eq. 6 as the ratio between m_a and m_w. Equation 7 expresses the abrasive velocity v_a at the focusing tube's exit, using a momentum balance between m_w, m_a and the mixed jet. Equation 8 shows the expression of P_{part}, which considers the abrasive as the only phase of the mixed jet that contributes to the material removal process, in AWJC.

$$v_{th} = \sqrt{\frac{2p}{\rho}} \tag{1}$$

$$v_{th,c} = \sqrt{\frac{2L}{\rho(1-C)}\left[\left(1+\frac{p}{L}\right)^{1-C}-1\right]} = \psi v_{th} \tag{2}$$

$$v_j = c_v v_{th,c} = c_v \psi v_{th} \tag{3}$$

$$Q_w = S_j v_j = c_c S_n v_j = c_c S_n c_v \psi v_{th} = c_d S_n v_{th} \tag{4}$$

$$m_w = \rho Q_w = \rho c_d S_n v_{th} \tag{5}$$

$$r_d = \frac{m_a}{m_w} \tag{6}$$

$$v_a = \frac{v_j}{1+r_d} \tag{7}$$

$$P_{part} = \frac{1}{2} m_a v_a^2 \tag{8}$$

3 Materials and methods

3.1 Equipment

The AWJC apparatus used in the present investigation is an Intermac Primus 322 Metal, installed at the Department of Mechanical Engineering of Politecnico di Milano (Italy). Its technical details are reported in Table 1. The cutting head is shown in Fig. 2. The experimental campaign has been carried out by using 75-mm focusing tubes (Ceratizit Premium Line design) and a Barton Garnet, mesh #80 abrasive.

Equations 1 through 8 can be applied to the present installation. The result can be appreciated in Figs. 3 and 4, which show the P_{part} theoretical trends versus p and m_a, respectively (step increases of 1 MPa and 1 g/min were used in the numerical computations). Both trends can be approximated as linear within the considered operational ranges.

The AWJC airborne acoustic emission has been measured by means of a PCB 130D20 condenser microphone, whose technical details are reported in Table 2. The microphone is shown in Fig. 5: it is installed on the cutting head and at a safe distance from the jet impinging point, to avoid possible damages from the backscattering of water and abrasive, thus providing adequate robustness to the setup. The microphone delivers a flat response up to 15 kHz; the sensitivity declines at higher frequencies, preventing its usage in the ultrasonic range (> 20 kHz) for quantitative measurements. Yet, the present application does not require a quantitative assessment of acoustic pressure, but only its qualitative correlation to a target variable; hence, the following processing methods have been applied up to higher frequencies, with respect to the microphone's flat response range.

The acquisition module is a National Instruments PXI including six Sound and Vibration modules PXIe-4492, with eight channels each and a maximum sampling frequency of 102.4 kHz.

Table 1 Technical specification Intermac Primus 322 Metal

Pressure intensifier	Power	37 kW
	Max p	380 MPa
	Max m_w	3.5 l/min
Handling system	5-axis cutting head	
	Longitudinal stroke	3210 mm
	Transversal stroke	2000 mm
	Vertical stroke	200 mm
Cutting head	Primary orifice d_n	0.33 mm
Focusing tubes	Inner Ø	1.02 mm
	Outer Ø	7.14 mm
	Length	75.0 mm or 101.0 mm
	Mass	60.3 g
	Material	Tungsten carbide

Fig. 2 Cutting head

3.2 Factorial tests

A first set of experimental tests has been intended to investigate the correlation of the airborne acoustic emission measured by the microphone with P_{part}. To the scope, four factorial test designs have been developed; these are reported in Table 3 and consist of two p set points (330 MPa, 380 MPa) and two m_a set points (300 g/min, 350 g/min). In the first test (Test 1), p has been maintained constant at 330 MPa and m_a varied according to a randomized sequence, with ten replicates at 300 g/min and ten replicates at 350 g/min. The second test (Test 2) is analogous to the first one, but here p is maintained constant at 380 MPa. In the third test (Test 3), m_a has been maintained constant at 300 g/min and p varied according to a randomized sequence, with ten replicates at 330 MPa and ten replicates at 380 MPa. The fourth test (Test 4) is analogous to the third one, but here m_a is maintained constant at 350 g/min. A total number of 80 tests has been carried out. In fact, this experimental campaign can be seen as a full-factorial plan with two factors (p and m_a) varying on two levels (330 MPa and 380 MPa for p and 300 g/min and 350 g/min for m_a), where the experiments' randomization has been blocked. The studied variations of p and m_a are kept relatively small as the purpose of this paper is to show the sensitivity of the proposed approach to parameters' variations that could depend on typical drifts happening as a consequence of components' wear or malfunctioning.

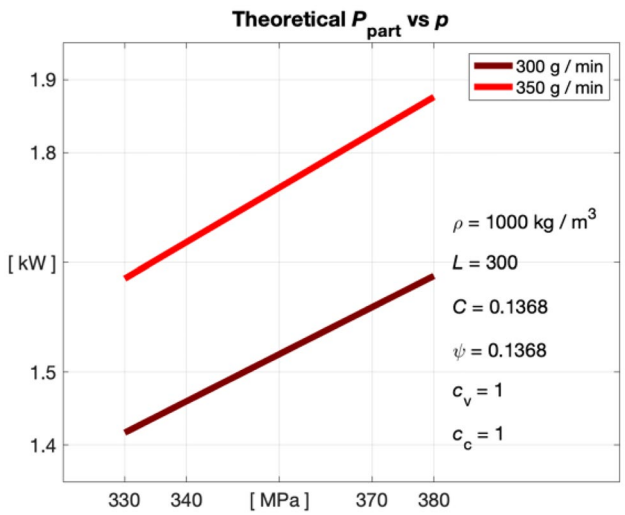

Fig. 3 Theoretical P_{part} vs p

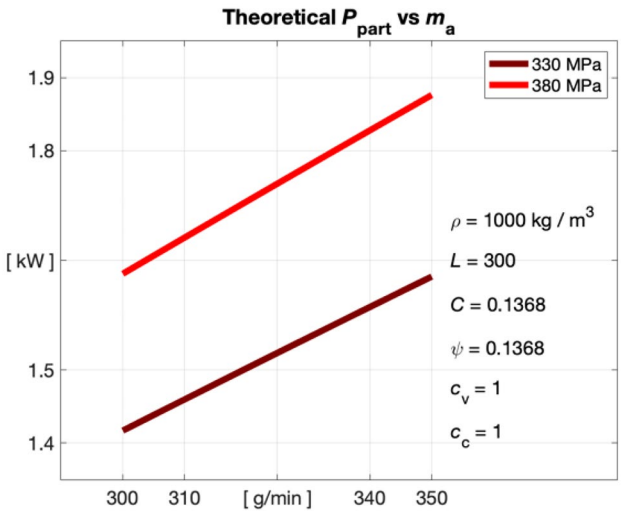

Fig. 4 Theoretical P_{part} vs m_a

From a practical standpoint and as it will be pointed out in Sect. 4, these factorial tests can be envisaged as calibration procedures of a simple model translating the acoustic data into a P_{part} estimation.

3.3 Validation tests

Further tests have been included into the experimental plan, to validate the method. Each validation test included ten replicates, in which the jet has been repeatedly fired at a constant m_a and according to a randomized sequence of p set points, comprised within the 330–380-MPa range. The airborne acoustic emission has been acquired and processed by means of the calibration factors obtained from the previous tests. Subsequently, the values of P_{part} foreseen by the empirical model have been compared with the correspondent theoretical ones.

Table 2 Technical specification PCB 130D20

Model	PCB 130D20 – ICP array microphone
Nominal diameter	1/4″
Frequency response (−2 to +5 dB)	20- to 15,000-Hz free-field
Sensitivity (at 1 kHz)	45 mV/Pa

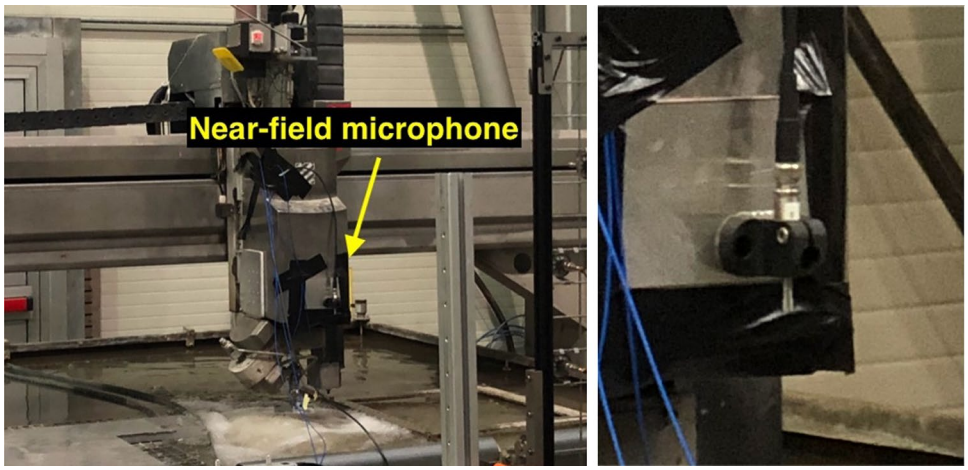

Fig. 5 Experimental setup and detail of the near-field microphone

Overall, the usage of randomized sequences during each test has been expected to compensate the impacts of drifts and interfering factors on the acoustic emission.

3.4 Methods

At each replicate, the jet has been fired for 5 s using the correspondent p and m_a set points, without workpiece and the head maintained in a steady position. In general, the head position has been maintained fixed throughout each test. After each test, the AWJC machine has been turned off; hence, each test has required the machine start-up and a reset of the handling system, resulting in different head positions amongst different tests. This procedure is useful to assess the method reproducibility in a real-case scenario.

At each replicate, the microphone's signal has been acquired using the following parameters: sampling frequency 102.4 kHz, sampling period 5 s, trigger level 0.1 V and pre-trigger 0.1 s. The waterjet cutting head has been switched on at every test making sure that the abrasive was already present in the hose, which makes transients negligible.

The signal processing has included a Welch's estimate of its power spectrum [27] using the following parameters, unless stated otherwise: segments of 0.01 s, hamming window and no overlap between adjacent segments. A further processing step consists in the computation of the power spectrum integral on a pre-defined frequency range.

Table 3 Factorial tests

	P (MPa)		m_a (g/min)	
Test 1	330		300	350
Test 2	380		300	350
Test 3	330	380	300	
Test 4	330	380	350	

The following notes of guidance throughout the results should be considered: the shown signals have not been scaled by the microphone sensitivity reported in Table 2.; hence their physical quantity is volt (V). Indeed, the aim of this investigation is not a quantitative assessment of the acoustic pressure, but only its qualitative correlation to a target variable. In the frequency domain, the power spectra have been expressed either in mV or decibel (dB). In the latter case, a dB reference of 2e − 5 V has been used. It follows that the units of the power spectrum integrals are mV·Hz.

4 Results

Before dealing with the present results, it is useful to look at conclusions from [5]: here, high-frequency data (above 10 and up to 50 kHz) was found to correlate with P_{part}; in particular, linear relations were found between the power spectra's integrals in such range and both p and m_a. Hence, analogous results are expected in the present investigation, given the physical relation existing between the structural vibration and the airborne acoustic emission, with the benefit of a more user-friendly monitoring setup that does not rely on contact sensors.

The top plot of Fig. 6 shows the near-field microphone's signal during a 5-s jet firing, in the time domain. The 0.1-s pre-trigger is evident, in the initial portion. The bottom plot of Fig. 6 shows the spectrogram of the time signal, which has been computed by using segments of 0.1 s, hamming window and no overlap between adjacent segments. The signal appears reasonably steady, except for a brief transient period of about 0.5 s immediately following the jet firing, in which contributions at low frequency (< 5 kHz) tend to rapidly disappear. Hence, the Welch's method can be licitly exploited for esteeming the signal's power spectrum, given its steadiness during the firing period.

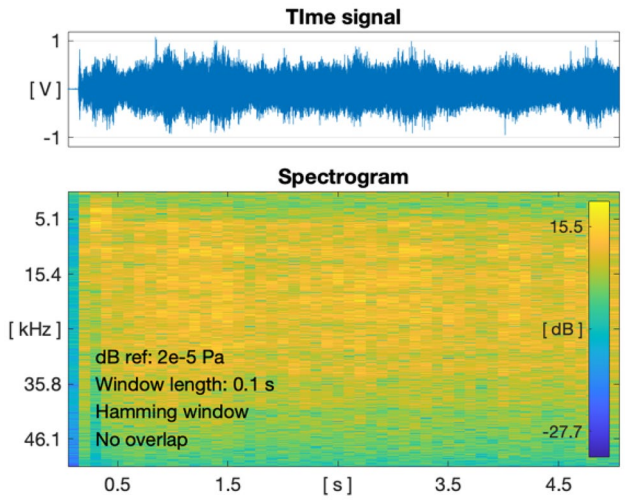

Fig. 6 Microphone's signal during jet firing

4.1 Background noise characterization

A comparison of signals gathered before and during the jet firing is important, to characterize the background noise and identify the eventual presence of further acoustic sources, besides the jet itself. To the scope, the signal of Fig. 6 has been divided into two parts: the first chunk of 0.1 s, in which the jet is not fired yet, and the remaining chunk of 4.9 s, in which the jet is fired throughout the entire period. In a subsequent step, the Welch's estimates of the two chunks have been computed, by using segments of 0.1 s, hamming window and no overlap between adjacent segments. The results are shown in Fig. 7: here the black and red curves correspond to the jet off and on, respectively. According to these results, the waterjet appears to dominate the overall measurement, with respect to other background sources (notably the pump, which is on throughout the entire acquisition period), especially at high frequency. Hence, the microphone's data can be licitly taken as a jet acoustic signature, relatively unaffected by further acoustic sources besides the jet itself. The acoustic signature is expected to characterize the jet robustly and selectively, by carrying a set of in-line information, possibly including P_{part}.

4.2 Factorial tests

Hereafter, the results of the factorial tests are presented, which are intended to assess the correlation of the acoustic measurements with P_{part} and extract calibration parameters that put the two quantities into relation. As the factorial tests provide measurements at different p and m_a set points, it is possible to investigate the separate effects of these two variables on the experimental data.

Firstly, the effect of m_a is addressed. To the scope, Test 1 includes ten replicates with m_a set at 300 g/min and other ten at 350 g/min, whilst p is maintained constant at 330 MPa. The Welch's estimates of the signals are shown in Fig. 8: here the light curves correspond to the single replicates; the dark curves correspond to the arithmetic averages, computed from the ten replicates at the correspondent m_a set point. Analogously, results for Test 2, in which p is maintained constant at 380 MPa, are shown in Fig. 9. These results indicate that m_a does not have a substantial impact on the acoustic data, neither at low nor high frequency.

Secondly, the effect of p is addressed. Figure 10 compares the curves from Test 3, in which m_a is maintained constant at 300 g/min and p varied between 330 and 380 MPa; an analogous comparison for Test 4, in which m_a is maintained constant at 350 g/min, is shown in Fig. 11. Contrarily to m_a,

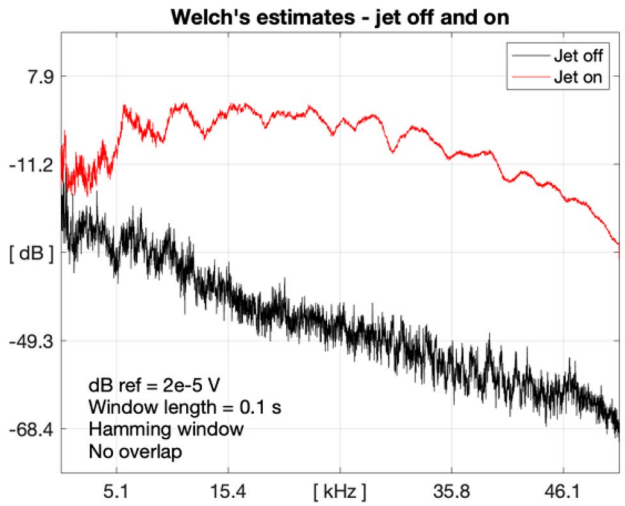

Fig. 7 Welch's estimates of the power spectra with jet off and on

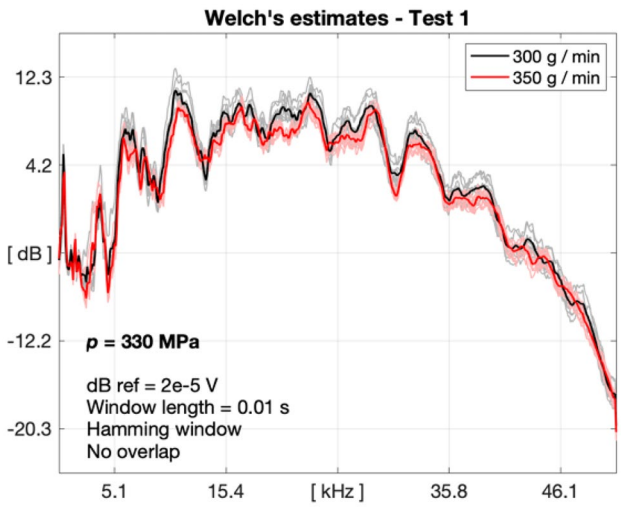

Fig. 8 Test 1. Light curves: single acquisitions. Dark curves: arithmetic averages

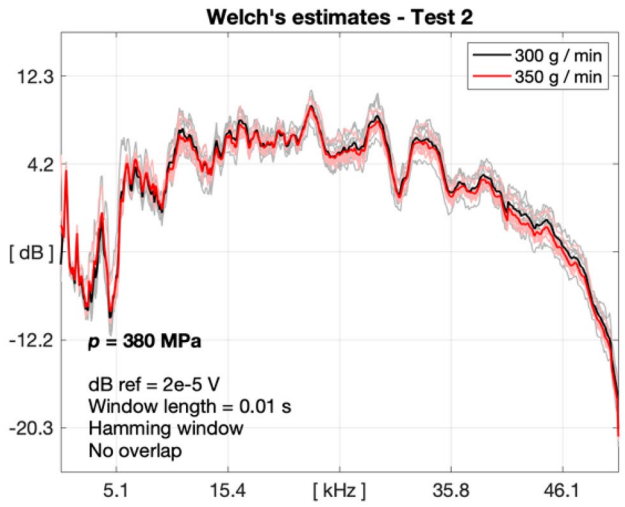

Fig. 9 Test 2. Light curves: single acquisitions. Dark curves: arithmetic averages

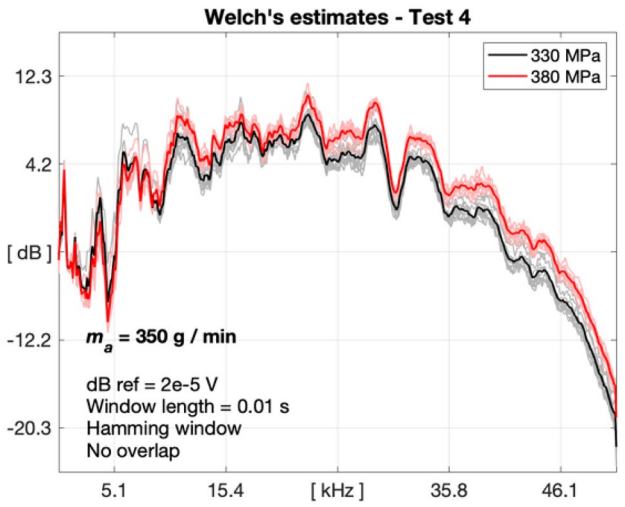

Fig. 11 Test 4. Light curves: single acquisitions. Dark curves: arithmetic averages

p has a detectable impact on the acoustic data, at high frequency: indeed, a clear separation amongst the two sets of curves appears in both tests, above 20 kHz. The separation does not occur, or at least is not as much evident, at lower frequencies.

Figure 12 shows the power spectrum integrals computed for the curves of Fig. 10, using the 10 Hz–10 kHz frequency range. Figure 13 shows analogous integrals for the curves of Fig. 11. In Figs. 12 and 13, the dots correspond to the single replicates, and the continuous lines are the mean values, each computed from the ten replicates at the correspondent set point. The areas correspond to the intervals of ± 1 standard deviation across the correspondent mean values. As it can be appreciated, there is no correlation between p and the acoustic data, in this frequency range.

On the other hand, Fig. 14 shows the power spectrum integrals computed for the curves of Fig. 10, using the 40–50-kHz frequency range. Figure 15 shows the analogous integrals for the curves of Fig. 11. This time a detectable separation amongst the two sets occurs, confirming a correlation between p and the acoustic measurements, at higher frequency.

One interesting comparison can be drawn amongst measurements from different tests, to assess the measurement reproducibility. On this regard, Figure 16 presents data gathered during various tests, at the $p = 330$-MPa set point (for the sake of clarity, only the averaged curves are shown). The total dataset includes tests at the two different m_a set points. However,

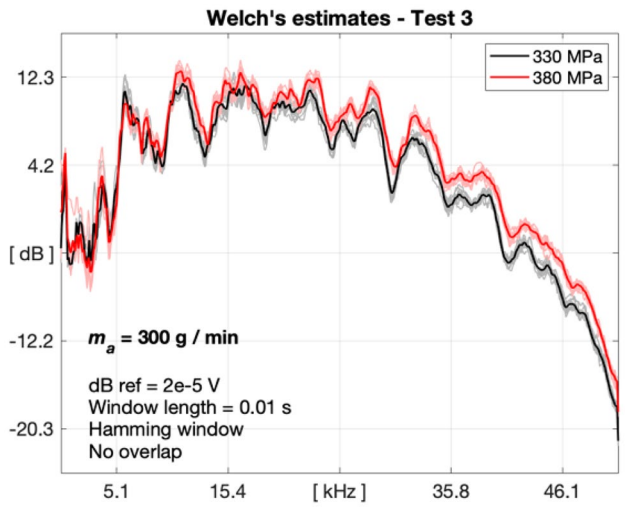

Fig. 10 Test 3. Light curves: single acquisitions. Dark curves: arithmetic averages

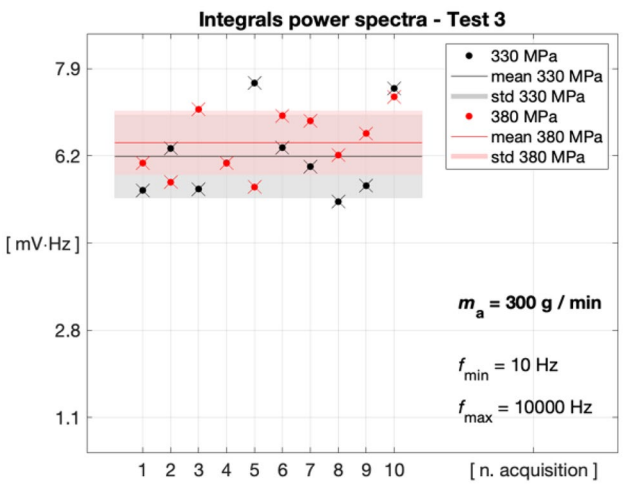

Fig. 12 Power spectrum integrals from Test 3. Frequency range = 10 Hz to 10 kHz

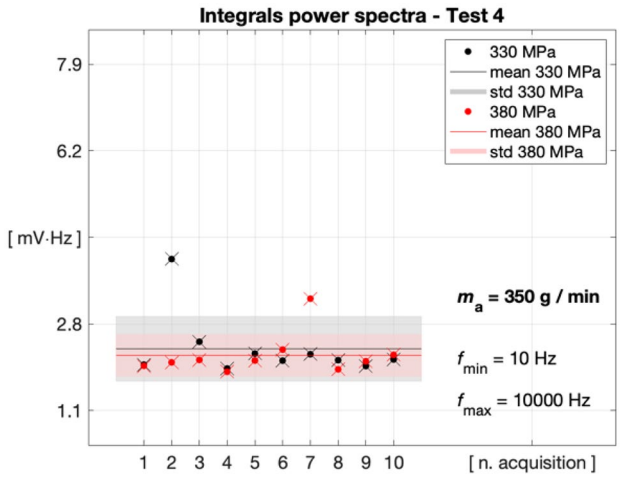

Fig. 13 Power spectrum integrals from Test 4. Frequency range = 10 Hz to 10 kHz

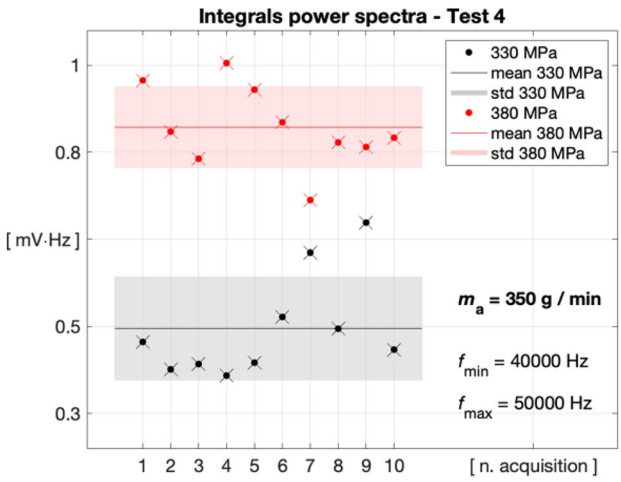

Fig. 15 Power spectrum integrals from Test 4. Frequency range = 40 to 50 kHz

this variable has already been proven to not have a substantial impact on the acoustic emission. Besides, the effect of further interfering factors occurring amongst different tests should be considered in the total measurement variability, as it has already been pointed out in Sect. 3.4. Figure 17 shows an analogous comparison for data gathered at the p = 380-MPa set point. In both cases, the spread amongst curves from different tests tends to reduce at high frequencies; above 40 kHz, it does not exceed 2 dB, indicating a good measurement reproducibility in such range.

As a note to the reader, it should be considered that contributions in such high-frequency range could be attenuated by the anti-aliasing filter of the acquisition module. However, the filter does not prevent the detection of p-induced effects on the same range, as proven in Figs. 10 and 11. Hence, the previous considerations on the measurement reproducibility are expected to remain valid, despite the filter's impact has not been characterized.

The good measurement reproducibility above 40 kHz is the discriminant factor for having chosen such value as the lower limit in the high-frequency analysis. The upper limit of 50 kHz is imposed by the Nyquist frequency (51.2 kHz), which comes from the adopted sampling frequency (102.4 kHz). Consequently, the low-frequency analysis has adopted a range from 10 Hz to 10 kHz, which disregards static contributions and provides an almost identical bandwidth.

Based on the results so far, a few conclusions can be drawn regarding the airborne acoustic emission: (1) data in the 40–50-kHz range corresponds to a robust and selective jet acoustic

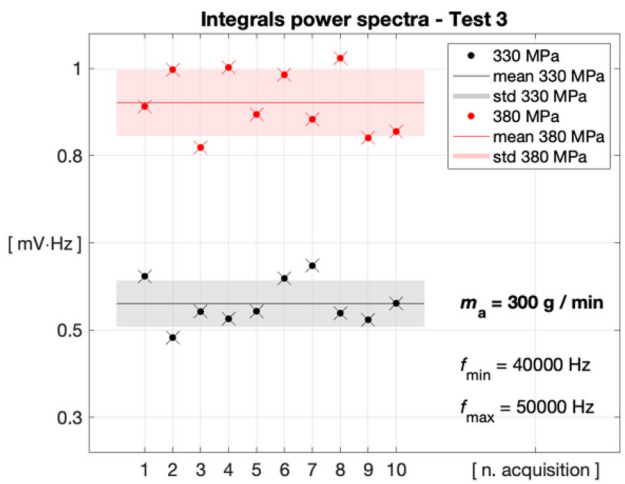

Fig. 14 Power spectrum integrals from Test 3. Frequency range = 40 to 50 kHz

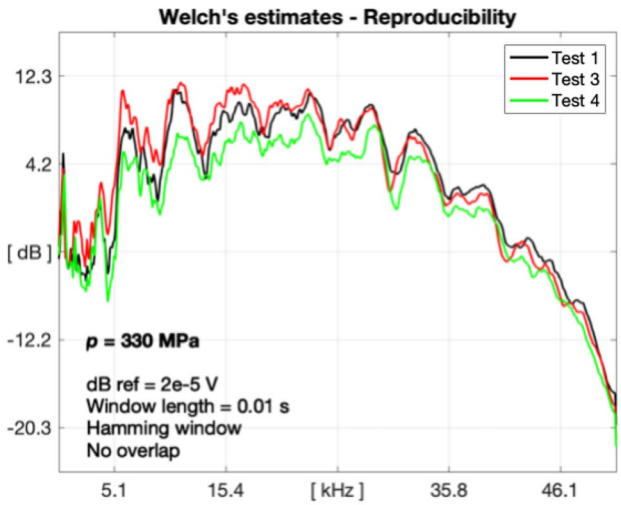

Fig. 16 Measurement reproducibility between different tests (only averaged curves) at p = 330 MPa

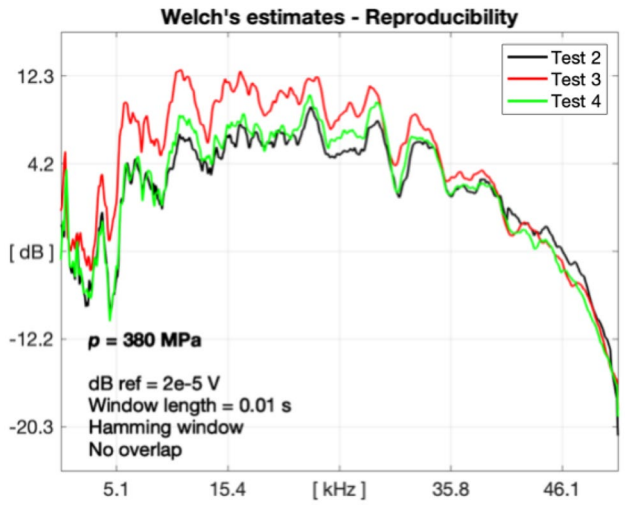

Fig. 17 Measurement reproducibility between different tests (only averaged curves) at $p = 380$ MPa

signature; (2) the acoustic signature appears not affected by background noise, input disturbances and interfering factors; and (3) the acoustic signature shows a detectable sensitivity to the p set point, whilst the m_a variations remain undetected. In conclusion, the acoustic signature seems capable of delivering a robust indicator of P_{part} and its p-induced variations, also providing a good measurement reproducibility amongst different test conditions.

4.3 Calibration procedure

Measurements from the factorial tests have been exploited for extracting factors that translate acoustic data into an estimated value of P_{part}. To the scope, it is useful to look at the theoretical trends of Figs. 3 and 4: as already pointed out, these can be assumed as linear in the operational ranges of this investigation. Hence, the transduction of acoustic data into a P_{part} index can be hypothesized in the form of Eq. 9, in which c_1 and c_2 are the two calibration factors and I is the experimental value, corresponding to the power spectrum integral in the 40–50-kHz range. The hypothesis assumes a linear correlation between P_{part} and I; this assumption will be the object of validation in the following subsection.

$$P_{part} = c_1 I + c_2 \tag{9}$$

One calibration can be done, by using data from Test 3: as the aim is computing the two unknown factors c_1 and c_2, two equations can be set by using the mean values of Fig. 14 as the I experimental values, and the correspondent P_{part} theoretical values. The result is presented in Fig. 18, which shows the fitting of the experimental values (red dots) against the theoretical trend (green line), after introducing the calibration factors. The calibration factors are reported, as well. One analogous calibration can also be done by using data from Test 4 at higher m_a, and the result is presented in Fig. 19. The calibration factors from the two tests are different; this is expected to be the direct consequence of the acoustic signature's unsensitivity to m_a. Hence, different calibration factors are required to fit the experimental values against the theoretical trends, where P_{part} is influenced by m_a too (Eq. 8).

4.4 Validation tests

Figure 18 also shows results for a validation test, in which ten replicates are carried out with m_a set at 300 g/min and p randomly varied amongst ten set points linearly spaced within the 330–380-MPa range; the black dots correspond to the experimentally foreseen P_{part} values, which have been computed by using the calibration factors from Test 3. An analogous validation test has been carried out with m_a set at 350 g/min and the correspondent results are shown in Fig. 19; here the experimentally foreseen P_{part} values have been computed by using the calibration factors from Test 4. The foreseen P_{part} values fit quite well the theoretical trends, in both cases.

An error can be computed, between each experimentally foreseen P_{part} value and the correspondent theoretical value. The mean error and the standard deviation of the foreseen P_{part} values with respect to the theoretical trends can be subsequently assessed, for both the validation tests. This statistical information is also reported in Figs. 18 and 19: the maximum mean error appears very limited, with respect to the nominal P_{part}, indicating a relatively low bias. The standard deviation of the method can be taken as the highest of the two values shown in Figs. 18 and 19 (0.016 kW) and corresponds to a 68.3% confidence interval (coverage factor equal

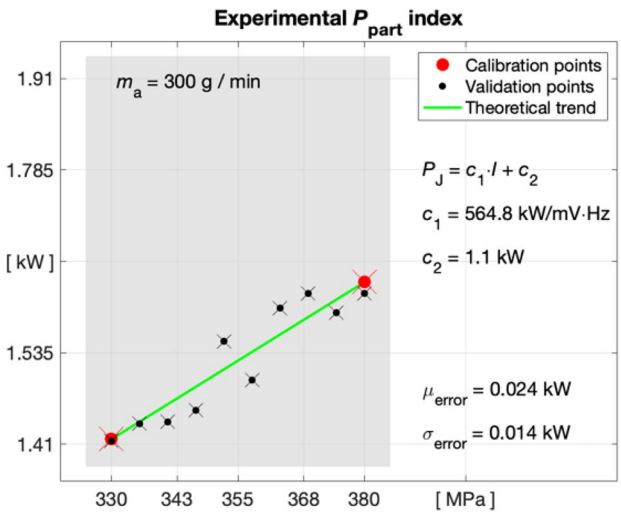

Fig. 18 Validation test at $m_a = 300$ g/min

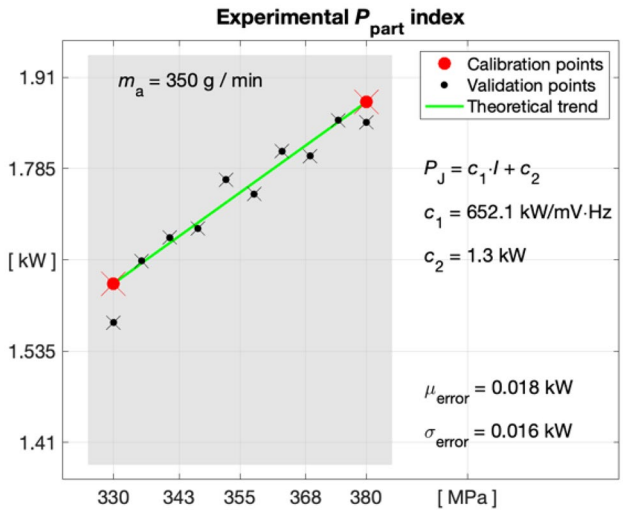

Fig. 19 Validation test at $m_a = 350$ g/min

to 1). In other words, a fluctuation of the experimentally foreseen P_{part} value equal to 0.016 kW can be associated to an actual variation of P_{part}, with a confidence level of 68.2%. By setting the target confidence level, it is possible to obtain the method's resolution, accordingly (Fig. 20).

The method presented in this paper enables an effective monitoring, tracking and control of the abrasive waterjet cutting capability. It is worth to remind that the present investigation has been carried out with the head steady and without cutting operations, as the head movement and the jet impingement on the workpiece were found to negatively affect the method's performance. Hence, a new operational stage can be envisaged, in which the waterjet is fired with the head steady and before attacking the workpiece; once the P_{part} index has been delivered, p can be retro controlled, if required. Subsequently, the machining operation can start.

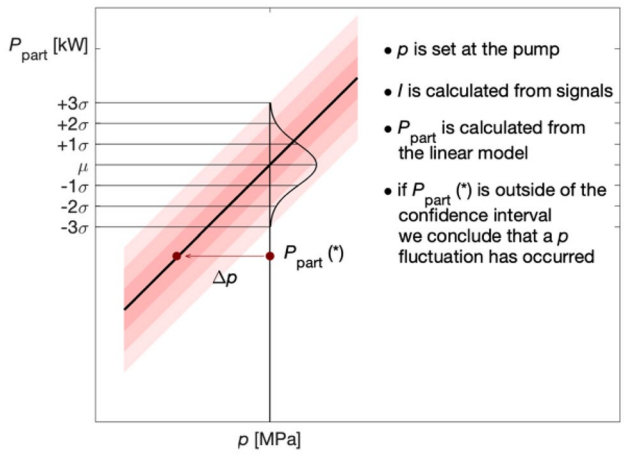

Fig. 20 Method's resolution

5 Conclusions

An experimental investigation has been carried out, addressing the correlation of the airborne acoustic emission of an abrasive waterjet cutting system with the jet kinetic power. Data above 40 kHz were found to constitute a robust and selective acoustic signature of the airborne jet, proven to be relatively unaffected by input disturbances and interfering factors, as well as relatively reproducible under different test conditions. The acoustic signature was found to be correlated with the jet kinetic power and its variations induced by the feeding water pressure, whilst variations induced by the abrasive feed rete remained undetected. A calibration procedure has been outlined, for computing factors that translate acoustic data into an in-line indicator of the jet kinetic power. Validation tests have been carried out by using theoretical definitions as benchmark, for comparison against the experimental indices. The proposed method appears effective in delivering a robust and accurate in-line indicator of the jet kinetic power and its pressure-induced variations. The method relies on a single microphone and appears more user-friendly with respect to prior-art setups that require contact sensors. The information delivered is expected to provide the ground for further investigations aimed at implementing innovative control strategies, particularly of the water pump, for improving the process stability.

Acknowledgements The authors would like to kindly acknowledge CERATIZIT Luxembourg S.à r.l. and Flow International Corporation for the fruitful discussions during the activity. The authors would like to kindly acknowledge CERATIZT Luxembourg S.à r.l. for having supported the SHIM project by providing specimens and consumables. The authors would like to acknowledge Dr. Francesco Perotti for the technical support provided throughout the experimental campaign.

Funding Open access funding provided by Politecnico di Milano within the CRUI-CARE Agreement. This work was supported by the project SHIM. The project has received funding under the JUMP Program of the Luxembourg National Research Fund (FNR), grant agreement no. PoC19/13599764/SHIM.

Declarations

Disclaimer The systems and methods for monitoring the operational vibration and delivering the power index from the signals are the objects of PCT and national patent applications [28–32]. The intellectual property included in said patents belongs to the University of Luxembourg. The Department of Mechanical Engineering of Politecnico di Milano provided the knowledge about the AWJC process and its physical description at the base of the theoretical definition of the jet power.

Competing interests The authors declare no competing interests.

Open Access This article is licensed under a Creative Commons Attribution 4.0 International License, which permits use, sharing, adaptation, distribution and reproduction in any medium or format, as long as you give appropriate credit to the original author(s) and the source, provide a link to the Creative Commons licence, and indicate if changes

were made. The images or other third party material in this article are included in the article's Creative Commons licence, unless indicated otherwise in a credit line to the material. If material is not included in the article's Creative Commons licence and your intended use is not permitted by statutory regulation or exceeds the permitted use, you will need to obtain permission directly from the copyright holder. To view a copy of this licence, visit http://creativecommons.org/licenses/by/4.0/.

References

1. Liu HT (2010) Waterjet technology for machining fine features pertaining to micromachining. J Manuf Proc 12(1):8–18. https://doi.org/10.1016/j.jmapro.2010.01.002.
2. Rabani A, Madariaga J, Bouvier C, Axinte D (2016) An approach for using iterative learning for controlling the jet penetration depth in abrasive waterjet milling. J Manuf Process 22:99–107. https://doi.org/10.1016/j.jmapro.2016.01.014
3. Annoni M, Arleo F, Viganò F (2017) Micro-waterjet technology. In: Fassi I, Shipley D, editors. Micro-Manuf Technol Their Applications. Springer Tracts Mech Eng 129–48
4. Hashish M (1989) Pressure effects in abrasive waterjet (AWJ) machining, Journal of Engineering Materials and Technology. Trans ASME 111(July 3):221–8. https://doi.org/10.1115/1.3226458
5. Copertaro E, Perotti F, Castellini P, Chiariotti P, Martarelli M, Annoni M (2020) Focusing tube operational vibration as a means for monitoring the abrasive waterjet cutting capability. J Manuf Process 59:1–10. https://doi.org/10.1016/j.jmapro.2020.09.040
6. Momber AW, Kovacevic R (2012) Principles of abrasive water jet machining. Springer Science & Business Media. https://doi.org/10.1007/978-1-4471-1572-4
7. Copertaro E, Perotti F, Annoni M (2021) Operational vibration of a waterjet focuser as means for monitoring its wear progression. Int J Adv Manuf Technol 116:1937–1949. https://doi.org/10.1007/s00170-021-07534-0
8. Hashish M (1994) Observations of wear of abrasive-waterjet nozzle materials. J Tribol 116(3):439–444. https://doi.org/10.1115/1.2928861
9. Hassan AI, Chen C, Kovacevic R (2004) On-line monitoring of depth of cut in AWJ cutting. Int J Mach Tools Manuf 44(6):595–605. https://doi.org/10.1016/j.ijmachtools.2003.12.002
10. Perzel V, Hreha P, Hloch S, Tozan H, Valícek J (2012) Vibration emission as a potential source of information for abrasive waterjet quality process control. Int J Adv Manuf Technol 61(1–4):285–294. https://doi.org/10.1007/s00170-011-3715-6
11. Valícek J, Hloch S (2010) Using the acoustic sound pressure level for quality prediction of surfaces created by abrasive waterjet. Int J Adv Manuf Technol 48(1–4):193–203. https://doi.org/10.1007/s00170-009-2277-3
12. Sutowski P, Sutowska M, Kaplonek W (2018) The use of high-frequency acoustic emission analysis for in-process assessment of the surface quality of aluminium alloy 5251 in abrasive waterjet machining. Proc Inst Mech Eng, Part B: J Eng Manuf 232(14):2547–2565. https://doi.org/10.1177/0954405417703428
13. Huaizhong L (2020) Monitoring the abrasive waterjet drilling of Inconel 718 and steel: a comparative study. Int J Adv Manuf Technol 107:3401–3414. https://doi.org/10.1007/s00170-020-05246-5
14. Karmiris-Obratańskia P, Karkalosa NE, Kudelskib R, Papazogloua EL, Markopoulosa AP (2021) Experimental study on the correlation of cutting head vibrations and kerf characteristics during abrasive waterjet cutting of titanium alloy. Procedia CIRP 101:226–229. https://doi.org/10.1016/j.procir.2020.11.011
15. Jurisevic B, Brissaud D, Junkar M (2004) Monitoring of abrasive water jet (AWJ) cutting using sound detection. Int J Adv Manuf Technol 24(9–10):733–737. https://doi.org/10.1007/s00170-003-1752-5
16. Hreha P, Radvanska A, Hloch S, Perzel V, Krolczyk G, Monkova K (2015) Determination of vibration frequency depending on abrasive mass flow rate during abrasive water jet cutting. Int J Adv Manuf Technol 77(1–4):763–774. https://doi.org/10.1007/s00170-014-6497-9
17. Popan IA, Bocanet V, Balc N, Popan AI (2018) Investigation on feed rate influence on surface quality in abrasive waterjet cutting of composite materials. In: Proc Int Conf Adv Manuf Eng Maters 105–13. https://doi.org/10.1007/978-3-319-99353-9_12. 18- 22 June 2018
18. Pahuja R, Ramulu M (2018) Abrasive waterjet process monitoring through acoustic and vibration signals. In: Proceeding of the 24th Conference on Water Jetting. ISBN: 5–7 September, 978–1–5108–7523–7524
19. Pahuja R, Ramulu M (2019) Surface quality monitoring in abrasive water jet machining of Ti6Al4V–CFRP stacks through wavelet packet analysis of acoustic emission signals. Int J Adv Manuf Technol 104(9–12):4091–4104. https://doi.org/10.1007/s00170-019-04177-0
20. Axinte DA, Kong MC (2009) An integrated monitoring method to supervise waterjet machining. CIRP Ann 58(1):303–306. https://doi.org/10.1016/j.cirp.2009.03.022
21. Rabani A, Marinescu I, Axinte D (2012) Acoustic emission energy transfer rate: a method for monitoring abrasive waterjet milling. Int J Mach Tools Manuf 61:80–89. https://doi.org/10.1016/j.ijmachtools.2012.05.012
22. Kovacevic R, Evizi M (1990) Nozzle wear detection in abrasive waterjet cutting systems. Mater Eval 48(3):348–353
23. Kovacevic R, Wang L, Zjang YM (1993) Detection of abrasive waterjet nozzle wear using acoustic signature. Proceedings of the American Waterjet Conference 7:217–232
24. Kovacevic R, Wang L, Zhang YM (1994) Identification of abrasive waterjet nozzle wear based on parametric spectrum estimation of acoustic signal. Proceedings of the Institution of Mechanical Engineers, Part B: J Eng Manuf 208(3):173–181. https://doi.org/10.1243/PIME_PROC_1994_208_076_02
25. Hreha P, Radvanská A, Cárach J, Lehocká D, Monková K, Krolczyk G, Ruggiero A, Samardzić I, Kozak D, Hloch S (2014) Monitoring of focusing tube wear during abrasive waterjet (AWJ) cutting of AISI 309. Metalurgija 53(4):533–536. ISSN: 0543- 5846
26. Jeong-Uk K, Roh-Won K, Sung-Ryul K, Hyun-Hee K, Kyung-Chang L (2022), Nozzle condition monitoring system using root mean square of acoustic emissions during abrasive waterjet machining. J Manuf Mater Proc 6 (31). https://doi.org/10.3390/jmmp6020031
27. Welch P (1967) The use of Fast Fourier Transform for the estimation of power spectra: a method based on time averaging over short, modified periodograms. IEEE Trans Audio Electroacoustics 15(2):70–3. https://doi.org/10.1109/TAU.1967.1161901
28. Copertaro E (2018) Wear monitoring device and process for an abrasive waterjet cutting head. Luxembourg national patent application No. LU100936. Filing date 26 September 2018
29. Copertaro E (2020) Wear monitoring device and process for an abrasive waterjet cutting head. PCT patent application No. PCT/EP2019/076119. Filing date 26 October 2019. Publication date 2 April 2020
30. Copertaro E (2018) Machining system and monitoring method. Luxembourg national patent application No. LU101065. Filing date 21 December 2018
31. Copertaro E (2020) Machining system and monitoring method. PCT patent application No. PCT/EP2019/086911. Filing date 23 December 2019. Publication date 25 June 2020
32. Copertaro E (2020) Waterjet focuser with DMS sensors for monitoring operational vibration and delivering an index of residual life. Luxembourg national patent application No. LU102298, filing date 16 December 2020

Publisher's Note Springer Nature remains neutral with regard to jurisdictional claims in published maps and institutional affiliations.